2019 Fourteenth International Conference on Ecological Vehicles and Renewable Energies (EVER)

A Holistic Approach for Simulation and Evaluation of Electrical and Thermal Loads in Lithium-Ion Battery Systems

Christoph Reiter*, Leo Wildfeuer, Nikolaos Wassiliadis,
Thilo Krahl, Johannes Dirnecker, Markus Lienkamp
Institute of Automotive Technology
Technical University of Munich
Boltzmannstr. 15, 85748 Garching, Germany
*Email: reiter@ftm.mw.tum.de

***Abstract*—Lithium-ion batteries (LIBs) exhibit a complex electrical and thermal behavior during operation. This is amplified at the system level, where the LIBs are arranged in a serial and parallel connection and phenomena such as parameter variations and heat transport effects exert additional influences that must be acknowledged and understood. Therefore, to reliably design battery systems with regard to safety and service life, a profound understanding of the exact behavior of each individual cell in the battery system is required. In this paper, the authors propose a holistic approach to model and simulate the complete electrical and thermal behavior of battery systems and a novel strategy to comparatively evaluate the load on individual cells. The modular design of the simulation framework allows fast adaptation to different battery interconnections and thermal properties. An analytic computation of the electrical and thermal effects ensures efficient computation. This enables investigations at both the cell and the system level, making it feasible to compare different system layouts systematically, including the consideration of additional influences like temperature sensors, cell balancing, and cooling systems or the environment. The electrical part of simulation framework is validated on the cell and the system level and an optimization-based approach for the parameterization of the thermal submodel is presented.**

I. Introduction

To ensure the suitability of a battery system design, the thermal and the electrical behavior on all system levels—down to the single cell—must be considered. Due to the high interdependence of the thermal and the electric battery behavior [1], neither side can be neglected. Furthermore, the behavior must be predicted over long periods of time, to ensure reliable operation for the whole service life. The result is a large simulation scope, associated with stringent demands on the computationally efficiency of the simulation.

To meet these demands in an efficient way, the authors propose a holistic framework that covers the requirements of electrical and thermal simulation and the evaluation of aging relevant load on the cell and the system level that can quickly be adapted to different battery systems and observation requirements. First, a theoretical consideration of lithium-ion battery (LIB) behavior, and a review on modeling approaches on the cell and the system level are carried out. Afterwards, the fundamental structure of the simulation framework is presented and the implementation of the electrical, thermal and load evaluation subroutines is explained. For quick comparison of different system designs without the need for time-consuming aging modelling, the paper introduces a novel, load-spectrum-analysis-based method to rank system stress factors.

The main contributions of the underlying publication can be summarized as follows:

- **Providing a computationally efficient model for current distributions within LIBs connected in serial and parallel:** An analytical approach for the calculation of current distribution inside parallel cell connections is deduced and described in detail. Based on the results, a matrix-based electrical battery system model is implemented enabling flexible and computationally efficient simulation of various battery pack configurations. The simulation framework is available for unrestricted use with an open-source license.
- **Introducing strategies for thermal modelling and monitoring on the cell and the system level:** Two approaches for thermal system simulation with different extent and complexity are presented and the demands for their parameterization, especially on the system level are discussed.
- **Contribute an approach for the evaluation of system loads:** A method based on load-spectrum analysis to evaluate electrical and thermal stresses for a given

battery system design and load cycles is derived, allowing transparent ranking of system load and detection of overloading.

- **Characterization and validation of the battery pack model:** Panasonic NCR18650PF LIBs with varying aging states are characterized alongside the experimental setup. Dynamic cell behavior and the influence of the measurement setup are separated by electrochemical impedance spectroscopy (EIS). Validation of the novel simulation approach is done for different load profiles.

The remaining paper is outlined as follows: In Section II, the theoretical background of LIBs and simulation on the cell and system level is discussed, including an extensive literature review of previous work in battery system simulation. In Section III, the simulation framework including the electrical, the thermal and the load evaluation submodel is presented. Section IV discusses the electrical and thermal validation of the simulation framework. The paper ends with a discussion and conclusion in Sections V and VI.

II. State of the Art

Modelling LIBs systems requires a comprehensive understanding of the effects occurring on the cell and the system level. Therefore, Subsection II-A gives a brief overview of single cell and cell-to-cell behavior and emphasizes the importance of considering both for designing battery systems in real world applications. In Subsection II-B and Subsection II-C, existing studies are revisited and their results briefly summarized. For further analysis of the results, subsection II-D introduces a method to evaluate cell load within the modelled battery system.

A. Lithium-Ion Batteries and Battery Systems

Under electric current load, LIBs show a characteristic dynamic voltage response, starting from their open-circuit voltage (OCV). This behavior is mainly influenced by the ohmic internal resistance of the LIB, as well as mass transport and double-layer effects [2] and is dependent on operating parameters like temperature, state-of-charge (SOC) and electric current rate (C-rate) [1]. The aforementioned factors all influence the magnitude of the LIB's aging process, which has influence on the operation parameters [3], [4].

One example is the rise of the ohmic internal resistance during the aging process, which leads to higher temperatures and consequently to a further acceleration of the aging processes. The closer LIBs are operated towards their operational limits, the faster degradation takes place. Therefore, a thorough understanding, prediction and monitoring of the so-called *stress factors*—influencing the cell's aging process—is necessary to predict the service life of LIBs in the later application [5]. In extreme cases, if LIBs are operated outside their specified operating range, short-term irreparable damage—and in the worst case—serious safety issues such as thermal runaway can occur [4].

For this reason, all relevant LIB operating parameters must be monitored at all times during usage and disconnected in the event of a fault, which is achieved in practice by the battery management system (BMS). To achieve this, critical thermal hot spots, if not avoidable, must be identified in advance and equipped with temperature sensors.

The complex interconnection between cell load, dynamic behavior, operating parameters like SOC and temperature as well as aging is further complicated as soon as individual LIBs are connected to a battery system. Due to slight differences in the electrical behavior of the individual cells and inhomogeneous temperature distributions within the system, the LIBs are exposed to different quantities of the individual stress factors and therefore might age differently [6]. A direct conclusion of this observation is, that due to the inhomogeneous distribution of electric current or temperature, individual cells are in danger of being overcharged [7], which might be hard to detect in the later application, when monitoring all parameters of every individual cell may be out of scope due to the high measuring and monitoring effort involved. Therefore, the battery system must be designed in a way that no excessive load imbalances occur and, if inevitable, are detectable by the BMS in the later application.

B. Electrical Battery System Simulation

In this Subsection, previous approaches for modeling the electrical behavior of parallel connected cells are reviewed and summarized in Table I. Since the majority of the literature is based on equivalent circuit models (ECMs), a widely popular modelling approach for LIBs—further explained in Subsection III-A—the focus lies on ECMs and their respective model complexity, parameterization methods as well as on validation procedures. The sorting of individual approaches is done based on the complexity of the ECM used.

Wu et al. [8] executed numerical simulations to analyze the behavior of parallel cells with different capacities during discharge. They did not use an actual ECM but chose the voltage-discharge capacity correlation at different C-rates to obtain the cells' voltage. For two parallel cells, they calculated the current distribution by an

TABLE I: OVERVIEW OF PREVIOUS PUBLICATIONS ON MODEL-BASED INVESTIGATIONS OF PARALLEL CONNECTED CELLS. **LEGEND:** -: NOT CONDUCTED; N/A: NOT AVAILABLE; ^{nP}: SEPARATE CURRENT TRACKING OF PARALLEL CONNECTED CELLS.

	Model			Parameterization		Validation	
Ref.	Type	Language	Topology	Measurements	Dependencies	Measurements	Evaluation
Wu [8]	Numerical	N/A	2p,3p	Discharges	C	-	-
Offer [9]	Semi-empirical	Simulink®	12p7s	Discharges	C	Discharge curves	Graphical
Spurret [10]	OCV + R_i	C++	2p	N/A	SOC, T	-	-
An [11]	OCV + R_i	MATLAB®	2p, 20p	DC-pulses, EIS	SOC	(Dis-)charges^{np}	Histogram, μ of error
Miyatake [12]	OCV + R_i	N/A	2s, 2p, 2s2p	Discharges	SOC	Discharge capacity	Numerical
Dubarry [13]	OCV + R_i + 1R||C	MATLAB®	1s2p, 1s3p	Discharges	C	Self-balancing^{np}	Graphical
Shi [14]	OCV + R_i + 1R||C	Simulink®	2p	(Dis-)charges^{np}	SOC	-	-
Gong [15]	OCV + R_i + 1R||C	Simulink®	2p	HPPC	SOC	Discharges^{np}	Graphical
Wang [16]	OCV + R_i + 1R||C	Simscape®	8p	(Dis-)charges	SOC,T,C	(Dis-)charges	Maximum error
Zhang [17]	OCV + R_i + 1R||C	Simscape®	3p3s	HPPC	SOC	FUDS	μ & σ^2 of error
Cordoba [18]	OCV + R_i + 1R||C	N/A	3s3p,3p3s	N/A	SOC, T, C	-	-
Fleckenstein [19]	OCV + R_i + 2R||C	Simulink®	3p	DC-pulse	SOC,T	Pulse Cycles^{np}	Graphical
Neupert [20]	OCV + R_i + 2R||C	N/A	4p	DC-pulses	SOC	Pulse Cycles^{np}	Graphical
Bruen [21]	OCV + R_i + 3R||C	N/A	4p	DC-pulses, EIS	SOC,T, C	Real driving cycle^{np}	Peak & RMS error
Brand [22]	OCV + R_i + 4R||C	N/A	2p	EIS	SOC	Impedance spectra	RMS error

iteration process using a binary search algorithm, however they did not validate their results with experimental data.

OFFER AT AL. [9] used the Simulink® SimPowerSystems battery model with semi-empirical equations to simulate a 12p7s battery pack. However, every cell was parameterized with the same discharge curves of one single cell and they only explored how abnormally high interconnection resistances affect the cells' response on a current interruption.

SPURRET ET AL. [10] developed a simple ECM containing a voltage source, internal resistance and leakage current in C++ to analyze the current distribution based on non-uniformity of two parallel connected cells, for which they could vary capacity and/or resistance to alter initial conditions of the strings. They state that they characterized their examined cell type extensively but did not give any information about their parameterization methods. Furthermore, results were not validated against experimental data.

AN ET AL. [11] studied charge/discharge characteristics of parallel connected cells and ultimately evaluated their sorting methods for newly manufactured cells with respect to block performance. They used an ECM containing an OCV and internal resistance, which was developed in MATLAB®. For a 2p-model, each cell was parameterized individually. They compared different DC-pulse and EIS parameterization methods for the internal resistance, gaining best results with the current interruption method. Verification of the model is achieved by constant current (CC) discharging of the parallel connected cells with separate current tracking. For a 20p-model, a Monte-Carlo method based on statistical data was used to assign the capacity values. The resistance value was then calculated using a negative correlation between capacity and resistance [11].

MIYATAKE ET AL. [12] experimentally investigated the influence of a battery configuration with non-uniform cells on the discharge capacity. They built an ECM consisting of a voltage source and internal resistance which they parameterized for two cells individually by CC discharge tests and performed simulations with up to 6 cells in parallel. However, they did not give further information on the model's capability of simulating the current distribution of parallel connected cells.

DUBARRY ET AL. [13] measured and simulated compensating currents of parallel connected cells in a 1s2p, 1s3p and a 2s2p topology using a single-cell ECM developed in MATLAB®. Parameters for one reference cell were obtained from discharge curves at different C-rates. Validation was performed by connecting cells with different SOC in parallel to provoke large compensating currents due to the self-balancing of cell voltages. The balancing currents were then calculated by a newly introduced method, where the ECM is used to calculate OCV curves at various C-rates and the transient current is obtained by scanning voltages to find where the sum of rates equals the assembly rates.

SHI ET AL. [14] developed a first order RC-model

for parallel connected cells in Simulink®. All in all, they gave very little detailed information about their modeling and parameterization methods. According to them, each branch current of the 2p-connection was calculated by a S-function solver in Simulink®. Branch parameters were then updated dependent on the SOC, which was determined by ampere-hour counting. They did not share the validation of their model at all.

GONG ET AL. [15] used Simscape® to connect two ECMs, each containing a voltage source, internal resistance and one RC element, in parallel. With differently degraded cells, they investigated inconsistent electrical behavior in parallel connections. Parameters were obtained for each cell separately. Results were validated against experimental data from measurements with separate current tracking while CC discharging.

WANG ET AL. [16] also implemented a first order RC-ECM using Simscape® and parameterized it by CC charge and discharge tests for 8 individual cells of the same type. They validated the voltage response of their single cell model and subsequently an 8p configuration. Furthermore, they simulated the current distribution within an 5p2s configuration to analyze the effect of an inconsistent cell, i.e. advanced aging. However, those simulation results were not benchmarked against experimental data.

ZHANG ET AL. [17] simulated the effect of internal resistance increase and capacity decrease on parallel connected cells by a first order ECM implemented again in Simscape®. With the high power pulse characterization (HPPC) and the federal urban driving cycle (FUDS), more dynamic profiles were used in order to parameterize and validate their pack model. However, only one parameter set was used for modeling a 3p3s-topology and neither simulations nor experiments regarding the current distribution were performed.

CORDOBA ET AL. [18] implemented a cell-model which contains a first order electrical, lumped element thermal and aging subsystem. This model was further expanded to pack level to simulate a 3p3s and a 3s3p topology using an analytical approach based on Kirchhoff's laws. They assumed capacity and internal resistance to be normally distributed and performed simulations on the influence of different initial cell-to-cell variability. Detailed information about parameterization methods was not presented, neither was a validation on cell level nor on pack level.

FLECKENSTEIN ET AL. [19] presented a thermal-electrical model with a second-order ECM (2 RC elements) for the electrical part. Their goal was to quantify inhomogeneities in three parallel connected cells on different temperature levels. Each cell model was parameterized identically. Due to temperature-dependent cell parameters, current imbalances present during a pulse profile could be simulated and experimentally validated.

NEUPERT ET AL. [20] implemented an electrical battery model based on a second-order ECM. For simulation of compensating currents in a 4p parallel connection, the cell models were extended using an analytical approach based on Kirchhoff's laws. The model was validated on the system level using current sensors for every individual cell. However, no thermal submodel was implemented, limiting the model's use to constant temperatures.

BRUEN ET AL. [21] developed an ECM with up to three RC elements for a single cell and expanded this cell model to a parallel connection of four cells including interconnection resistances. They investigated the current sharing in the parallel strings and resulting effects like inhomogeneous heating or charge throughput. Model parameters were identified for each cell individually by pulse power tests as well as EIS measurements. Lastly, they validated the simulated current distribution using a dynamic real-world driving cycle.

BRAND ET AL. [22] focused on intrinsic parameter differences, namely capacity and resistance, to investigate the current distribution within two parallel connected cells. Therefore, they implemented an ECM containing four RC elements. The cell ECM was individually parameterized via EIS measurements. Validation of the simulation results was done by CC pulses. Special emphasis was placed on a precise measurement setup with low additional impedance.

In the literature review, a large variety regarding model complexity, parametrization effort and validation methods can be observed. All in all, simplicity of the presented models correlates with their parametrization and validation methods. In some studies, a series connection of OCV and internal resistance was declared to be sufficient. It needs to be stated that these authors mostly performed CC charge or discharge measurements in the range of minutes for parameterization as well as validation. More dynamic effects, such as the influence of the solid electrolyte interphase (SEI) on the cell's impedance or charge transfer dynamics, cannot be captured with these approaches. In order to simulate the cell's response to dynamic load profiles, more accurate modeling of the cell's electric behavior and in particular more detailed parameterization is required. Therefore, one or multiple RC-elements are connected in series with the OCV and internal resistance. Amongst some of the reviewed modeling approaches, more dynamic validation methods,

such as the FUDS and real driving cycles can be found [21].

Currently, few publications have mentioned the exact implementation of the current distribution calculation within parallel connected cells. Physical based simulation tools like Simscape®often are employed, resulting in inflexible and computationally inefficient system models.

C. Thermal Battery System Simulation

For thermal simulations of battery systems, modeling LIBs as thermally connected lumped masses has proven to be a computationally effective way [18], with the cost of offering no information of the cells' internal temperature distribution. Temperature gradients inside individual cells have been shown to influence the overall LIB behavior and aging [23], but the simulation of this anisotropic heat transfer problem also requires in-depth knowledge of the exact internal structure of the LIB and the thermal properties of its components [24].

Consequently, the thorough validation of these models requires data of cell internal temperatures, which is not trivial to acquire for commercially available LIBs without intrusive testing. In general, the consideration of cell internal gradients can be assumed to be necessary only for operation under high Biot numbers conditions [25], per definition mostly present when operating with larger-format cells.

D. Evaluation of Battery Stress Factors

In Section II-A, the influences on and impact of LIB aging were explained. In order to establish the connection between stress factors and degradation, aging models are used. The spectrum ranges from data-driven approaches over phenomenological to electrochemical models, aiming to exactly simulate the processes inside the LIB [26]. Regardless of their type, all aging models have in common the high effort in their parameterization, which requires cell-specific, extensive and long-term testing and validation.

Since parameterization of performance-based aging models must be customized for every cell chemistry and type, comparing different system concepts in the early design phase, when there is still a large solution space, is a time-consuming task that cannot always be feasibly accomplished. One possibility to overcome this issue is the utilization of load-spectrum analysis, where the amplitude and frequency of relevant stress-factors and the combination thereof is monitored. This event-based approach allows an initial assessment whether a battery system is operated under aging-relevant or harmful operating conditions, enabling a qualitative comparison to other designs. In a next step, with additional testing effort, the events can be linked to their impact on cell aging [27].

III. Simulation Framework

Based on the theoretical assessment in Section II, this section derives the chosen approach of the simulation model. As a compromise between accuracy and computational effort, a joint approach of an electrical simulation based on an ECM and a thermal simulation based on lumped masses is chosen. The electrical and thermal properties of every individual LIB inside the battery system are monitored and represented through the possibility to either assign a unique parameter set to every cell, consideration of statistical deviations from expectation values or a combination thereof. The latter case is especially suitable for the modeling of fault scenarios or worst-case considerations.

For efficient scaling to different battery system sizes, all operating parameters inside the simulation framework are represented by two dimensional arrays. This matrix-based approach allows adaption to different LIB interconnections without changes to the code itself. The implementation is done in MATLAB®/Simulink®. All algorithms are designed for discrete calculation, based on the last time-step for efficient computation.

The simulation framework is structured into different submodels. The basic structure is shown in Figure 1. The framework is split into an electrical and a thermal subroutine, which are further segmented into the cell, the system and a monitoring level. All simulated operating parameters simulated are fed into the load-evaluation submodel for further evaluation.

The individual components of the simulation framework are explained in the following sections.

A. Electrical Simulation on the Cell Level

As discussed in the review in Subsection II-B, most of the publications use ECMs to simulate electrical cell behavior within parallel connections as a trade-off between accuracy and effort for implementation, parameterization and computation. The complexity of these models ranges from a single ohmic resistance representing an overall DC resistance [10]–[12] to more recent publications using models with three [21] or four RC elements [22] representing dynamic effects with various time constants.

In this study, an ECM with four RC elements as shown in Figure 2 is used as a compromise between accuracy

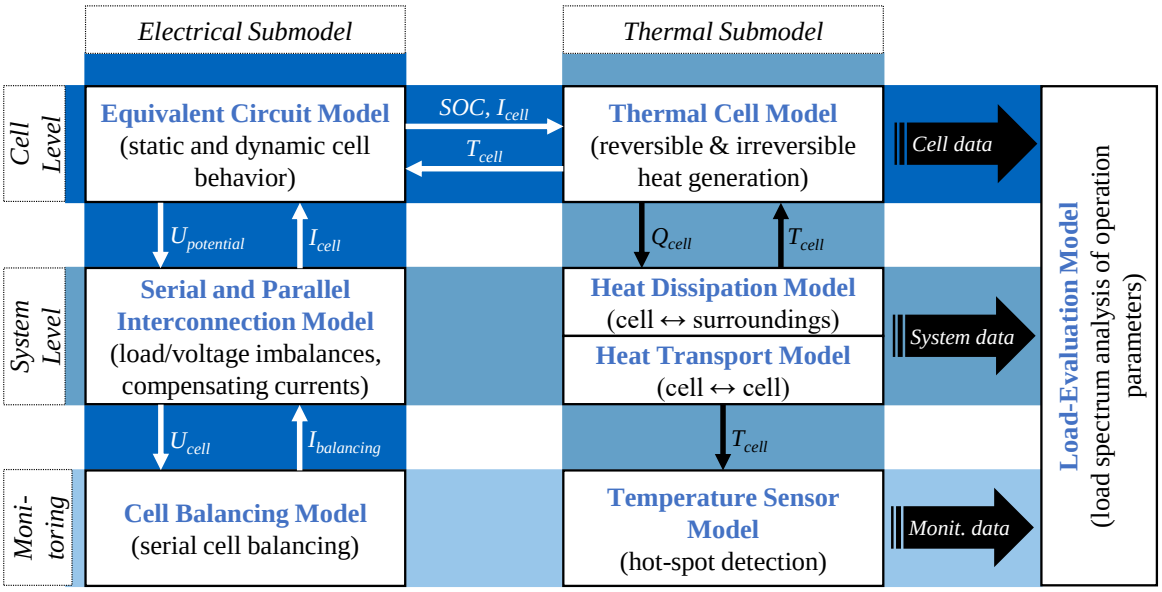

Fig. 1: Basic structure of the simulation framework.

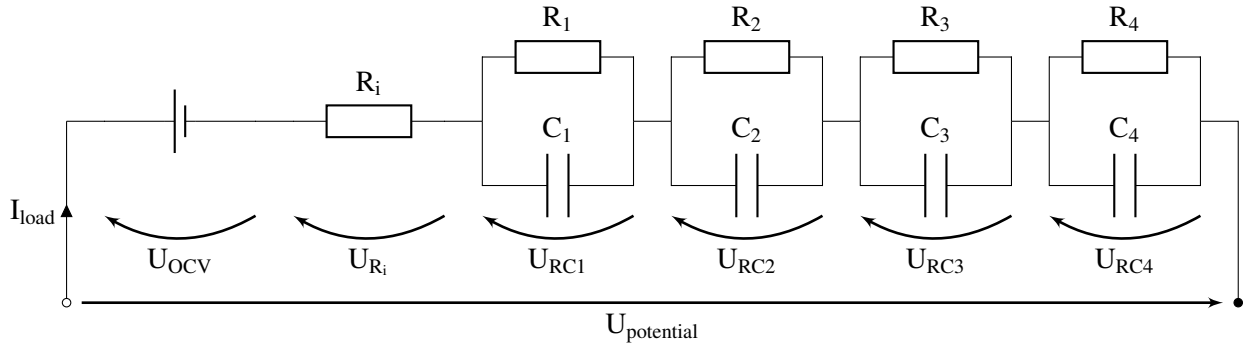

Fig. 2: Equivalent circuit model with four RC elements.

and computational and parameterization effort. In the time discrete domain and state-space representation, the dynamic part of the ECM can be expressed as

$$\mathbf{x}^{\star} = \begin{bmatrix} a_1 & & & 0 \\ & \ddots & & \vdots \\ & & a_4 & 0 \\ 0 & \dots & 0 & 1 \end{bmatrix} \mathbf{x} + \begin{bmatrix} R_1\,(1-a_1) \\ \vdots \\ R_4\,(1-a_4) \\ \frac{\Delta t}{C_N} \end{bmatrix} I_{cell} \quad (1)$$

with

$$\mathbf{x} = \begin{bmatrix} U_{RC1} & \dots & U_{RC4} & SOC \end{bmatrix}^T \quad (2)$$

and $\mathbf{x}^{\star}$ being the state vectors of the last respectively current time-step, U_{RCn} the over-voltage, R_n the resistance and C_n the capacity of the n-th RC element, SOC the cell's state of charge, defining the cell's respective open circuit voltage $U_{OCV}(SOC)$, C_N the nominal capacity, I_{cell} the current load, Δt the size of the discrete time-step and

$$a_n = \exp\left(-\frac{\Delta t}{R_n C_n}\right) . \quad (3)$$

Due to slight production fluctuations, every LIB in a battery system shows a slightly different dynamic behavior, depicted by an individual ECM parameterization. The simulation framework allows the allocation of independent ECM parameter sets to any desired cells. As an alternative solution, if an independent parameterization of all cells is not feasible, every ECM parameter can be complemented with a random, normally distributed shift according to its standard deviation. A combination of the methods is also possible.

The currents through the individual cells $I_{cell,j}$ are dependent on the external current load as well as the compensating currents in between the parallel cells. The calculation of $I_{cell,j}$ inside the parallel connection is explained in the following section.

B. Electrical Simulation on the System Level

The current distribution inside a parallel connection is caused by a complex interaction of the external load as well as the resistance, capacity and SOC of the individual LIBs. To compute this current distribution, previous publications discussed in Subsection II-B often used physical based simulation tools such as Simscape® or have not described their method of modeling compensating currents at all.

The limitation of tools like Simscape® was found in their strategy of representing every physical signal as a scalar value. Because of this, every component like a cell in parallel and/or serial connections of certain battery topologies needs its unique representation. Thus, simulations, especially of highly parallel connections lead to large and complex models. This makes the model inflexible, since an adjustment of the amount of cells requires changes in the model itself.

To overcome these limitations, a fully analytical approach based on Kirchhoff's laws, proven as effective by [18], [20], was developed and implemented in Simulink®. The model is able to adapt to different numbers of serial and parallel cells without any modeling changes due to its matrix-based implementation and allows a discrete time and efficient computation of compensating currents between parallel cells.

The following part describes the algorithm for the general case of a parallel circuit consisting of p cells using an ECM with n RC elements. For the case of $p = 1$ the parallel circuit model simplifies itself to that of a single cell, allowing the use of one model for nearly all purposes. The algorithm starts by calculating the electric potential $U_{potential,j}$ of every cell $j = 1, \ldots, p$. Using the ECM described in Subsection III-A, this is achieved by

$$U_{potential,j} = U_{OCV,j} + \sum_{n=1}^{q} U_{RCn} + U_{hysteresis,j} \quad (4)$$

with U_{OCV} being the open circuit voltage, U_{RCn} the voltage of the n-th RC element and $U_{hysteresis}$ the hysteresis voltage, implemented according to Verbrugge et al. [28].

In order to calculate the theoretical short-circuit current $I_{short\text{-}circuit,j}$ of every cell, the equivalent circuit is simplified to a voltage source with the ohmic internal resistance R_i

$$I_{short\text{-}circuit,j} = \frac{U_{potential,j}}{R_{i,j}} \ . \quad (5)$$

The sum of all short circuit currents $I_{short\text{-}circuit,j}$, together with the external load current I_{load}, gives the—again theoretical—total current I_{total} through the whole parallel connection.

$$I_{total} = \sum_{j=1}^{p} I_{short\text{-}circuit,j} + I_{load} \quad (6)$$

Utilizing the total equivalent internal resistance

$$R_{total} = \left(\sum_{j=1}^{p} \frac{1}{R_{i,j}} \right)^{-1} \quad (7)$$

I_{total} allows calculating the voltage U_{total} of the parallel connection.

$$U_{total} = R_{total} \ I_{total} = U_{cell,j} \quad (8)$$

In parallel connections this is equal to the voltage of all cells in the connection $U_{cell,j}$. Together with the electric potential $U_{potential,j}$ from equation (4) the voltage across the ohmic resistance of the single cells

$$U_{R,j} = U_{cell,j} - U_{potential,j} \quad (9)$$

can be calculated and used to determine the individual current

$$I_{cell,j} = \frac{U_{R,j}}{R_{i,j}} \quad (10)$$

through each cell. This current includes the compensating currents between the cells as well as currents originating from external load. This can be verified by

$$\sum_{j=1}^{p} I_{cell,j} = I_{load} \quad (11)$$

since the sum of the currents through the single cells always equals the external load.

The fully analytic algorithm presented here is capable of discrete execution without continuous states. Therefore, no numerical solution of differential equations is necessary, making the algorithm computationally efficient and suitable for the simulation of even large battery systems. The analytical approach promises general validity for any number of parallel cells. Since the variables can be implemented as arrays, the algorithm can adapt to other cell numbers without changing the model or code.

The arrays can also be extended to matrices, allowing the additional simulation of serial connections. If statistic deviations of cell properties are used, the serial elements in the battery system, like in real applications, will become unbalanced over time, resulting in voltage drift and a limited usable capacity. To address these demands, a submodel allowing dissipative cell balancing was implemented. For every serial element i a balancing current

$$I_{bal,i} = -\frac{U_{total,i}}{R_{bal}} \tag{12}$$

defined by the balancing resistor R_{bal} and the voltage of the serial element $U_{total,i}$ is calculated. Basic voltage- and current-based criteria for cell balancing can be defined in model parameterization. However, due to the modular approach, it is also possible to easily implement more advanced balancing algorithms.

C. Basic Thermal Simulation

Since the electrical parameters of lithium-ion cells are temperature dependent [2], it is necessary to simulate the cells' temperatures and adjust the parameters accordingly. Consequently, a thermal submodel was implemented to calculate the temperature of every single cell.

The thermal submodel derivates the cell-individual heat release from the voltage losses calculated in the ECM. Since the cells are assumed as lumped masses, inner temperature gradients are disregarded. As a further simplification, it can be assumed in the first step that there is no heat conduction between the cells and every cell only exchanges thermal energy with its ambient temperature over a specified portion of its surface area and a heat transfer coefficient. For this assumption, in theory, no further geometrical information about the battery system is necessary.

In order to determine the temperature of the cells which are regarded as lumped masses with uniform temperature, the balance of heat generation inside every cell $\dot{Q}_{cell,j}$ and heat transfer between cell and environment $\dot{Q}_{\infty,j}$ must be calculated. For the cell's heat generation, irreversible and reversible losses are modeled according to [29] as seen in equation (13). The irreversible part is caused by the sum of overvoltages $U_{R,j}$ at the RC elements and the internal resistance $R_{i,j}$. The reversible part, originating from chemical effects in the cell's active material, depends on current, temperature $T_{cell,j}$ and an entropy coefficient $\frac{\partial U_{OCV,j}}{\partial T_{cell,j}}$ of the cell.

$$\dot{Q}_{cell,j} = \overbrace{U_{R,j}\ I_{cell,j}}^{\text{irreversible heat}} + \overbrace{I_{cell,j}\ T_{cell,j}\ \frac{\partial U_{OCV,j}}{\partial T_{cell,j}}}^{\text{reversible heat}} \tag{13}$$

Since the heat transfer between a cell and its environment is assumed to be conductive in nature only, the heat transfer is defined by only a heat transfer coefficient $\alpha_{cell,j}$, the cell's surface A_{cell} and temperature $T_{cell,j}$ as well as the environmental temperature $T_{\infty,j}$ around the cell.

$$\dot{Q}_{\infty,j} = \alpha_{cell,j}\ A_{cell}\ \ (T_{\infty,j} - T_{cell,j}) \tag{14}$$

For efficient implementation in the simulation framework equation (14) is transformed to matrix notation which, for n cells, yields

$$\begin{bmatrix} \dot{Q}_{\infty,1} \\ \vdots \\ \dot{Q}_{\infty,n} \end{bmatrix} = \underbrace{\begin{bmatrix} \frac{1}{R_{\alpha,1}} & & 0 \\ & \ddots & \\ 0 & & \frac{1}{R_{\alpha,n}} \end{bmatrix}}_{\mathbf{K}_\infty} \left(\begin{bmatrix} T_{\infty,1} \\ \vdots \\ T_{\infty,n} \end{bmatrix} - \begin{bmatrix} T_{cell,1} \\ \vdots \\ T_{cell,n} \end{bmatrix} \right) \tag{15}$$

with $R_{\alpha,n}$ as thermal transfer resistance, defined by

$$R_{\alpha,j} = \frac{1}{\alpha_{cell,j}\ A_{cell}} \tag{16}$$

and $\mathbf{K}_\infty$ as thermal resistance matrix. If the battery system or individual cells are cooled by forced convection, $\alpha_{cell,j}$ may not be static as it must be adjusted depending on the operating conditions of the cooling system [30].

The total thermal balance of a cell $Q_{total,j}$, with respect to the discrete time-step Δt, is calculated by

$$Q_{total,j} = \left(\dot{Q}_{cell,j} + \dot{Q}_{\infty,j} \right) \Delta t\ . \tag{17}$$

$Q_{total,j}$ describes the change of thermal energy inside the cell since the last time-step and is used to calculate the new temperatures

$$T^{\star}_{cell,j} = \frac{Q_{total,j}}{m_{cell,j} c_{cell,j}} + T_{cell,j} \tag{18}$$

dependent on the temperatures $T_{cell,j}$ from the last timestep and the cell's mass $m_{cell,j}$ and heat capacity $c_{cell,j}$.

This method intentionally neglects effects like free and forced convection, thermal radiation or heat conduction between the cells because these are difficult to determine and are potentially unknown when using the model in the design phase of a battery pack. However, by assigning individual heat transfer coefficients $\alpha_{cell,j}$ gathered from

experimental data, these effects can be accounted for, at least phenomenologically. Therefore, the chosen approach does not require the high effort of identifying, modeling and parameterizing all present mechanisms of heat transfer and in specific cases the achieved accuracy can be regarded as sufficient.

D. Heat Transfer Between Individual Cells

In many cases, however, the heat transfer between the individual cells must be considered [31]. This requires the availability of three-dimensional geometrical information of the battery pack as well as the thermal interaction specific to each cell type.

Considering the symmetry of heat transport and heat resistance the total heat flux $\dot{Q}_{\lambda,j}$ for a cell j in thermal contact with n other cells can be calculated by

$$\dot{Q}_{\lambda,j} = -\frac{T_{cell,j}}{\sum_n R_{\lambda,jn}} + \sum_n \frac{T_{cell,n}}{R_{\lambda,jn}} \tag{19}$$

with $R_{\lambda,jn}$ as the thermal resistance between the cells j and n. Equation (19) can be generalized for all n cells which—using matrix notation—yields

$$\begin{bmatrix} \dot{Q}_{\lambda,1} \\ \vdots \\ \dot{Q}_{\lambda,n} \end{bmatrix} = \underbrace{\begin{bmatrix} -\frac{1}{\sum_n R_{\lambda,1n}} & \frac{1}{R_{\lambda,12}} & \cdots & \frac{1}{R_{\lambda,1n}} \\ & \ddots & \ddots & \vdots \\ & & \ddots & \frac{1}{R_{\lambda,(n-1)n}} \\ & & & -\frac{1}{\sum_n R_{\lambda,nn}} \end{bmatrix}}_{\mathbf{K}_\lambda} \begin{bmatrix} \dot{T}_{cell,1} \\ \vdots \\ \dot{T}_{cell,n} \end{bmatrix} \tag{20}$$

with the symmetric heat transfer matrix $\mathbf{K}_\lambda$. The additionally considered heat transfer $\dot{Q}_{\lambda,j}$ between the cells thus extends equation (17) to

$$Q_{total,j} = \left(\dot{Q}_{cell,j} + \dot{Q}_{\infty,j} + \dot{Q}_{\lambda,j}\right) \Delta t \tag{21}$$

omitting the simplification of an only convective heat dissipation used in Subsection III-C.

The usage of the heat transfer matrix $\mathbf{K}_\lambda$ offers the possibility to model heat flux between all LIBs in the battery system. To reduce the complexity in parameterization, in the first step, it is advisable to use the principle of thermal networks and only consider heat fluxes between adjacent cells. The simulation framework offers the possibility to automatically set up $\mathbf{K}_\lambda$ if the heat conduction resistances in all three spatial directions are specified. In reality, however, there will be also heat fluxes via module and system housings and electrical wiring which must be considered, if high accuracy is required. A process to parameterize the thermal submodel is discussed in Subsection IV-D.

In the simulation framework's current implementation, the cells are represented as lumped thermal masses, so the number of entries in $\mathbf{K}_\lambda$ is equal to the number of physical LIBs in the simulated battery system. If the assumption of lumped masses is not valid, it is theoretically possible to represent individual LIBs with more entries in $\mathbf{K}_\lambda$, allowing the simulation of inner-cell thermal gradients. However, due to the expected high impact on computation time this strategy is currently not being pursued.

E. Stability of Thermal Simulation

The discrete computation offers significant advantages in terms of computation time, especially for large time-steps Δt. However, if Δt is chosen too large, the simulation will get unstable and return inaccurate results. Thus, it must be determined, if the chosen Δt allows for a stable simulation.

To achieve this, the full equation solved by the thermal submodel must be considered. It can be obtained by combining equations (13), (15), (18), (20) and (21) which, in matrix notation, yields

$$\mathbf{T}^\star_{cell} = \underbrace{\left(\mathbf{E}_n + \frac{\Delta t}{m_{cell} c_{cell}} \cdot (\mathbf{K}_\lambda - \mathbf{K}_\infty)\right)}_{\mathbf{A}} \mathbf{T}_{cell} + \\ + \frac{\Delta t}{m_{cell} c_{cell}} \cdot \left(\dot{\mathbf{Q}}_{cell} + \mathbf{K}_\infty \mathbf{T}_\infty\right) \tag{22}$$

with $\cdot$ depicting line-by-line multiplication. The simulation is stable, if the condition

$$|\operatorname{eig}(\mathbf{A})| \leq 1 \tag{23}$$

is fulfilled. This allows the simulation framework to either test, if the thermal simulation is stable for a given Δt, or search for the largest possible Δt using the bisection method.

F. Temperature Monitoring

The simulation of all properties for every single cell produces large amounts of logging data. Also, due to cost restrictions in real applications, not every individual LIB's temperature is monitored. Therefore, a temperature sensor submodel is included in the simulation framework.

The submodel allows the aggregation of one or more cell temperatures to any desired number of sensor value. The sensors can either be defined by manually selecting all cells constituting the sensor or by specifying a measuring

TABLE II: COMPARISON OF LOGGING DATA SIZE BETWEEN STANDARD TIME-SERIES AND LOAD SPECTRUM ANALYSIS.

Number of logged system variables	Method	$t_{sim} = 2000s$	$t_{sim} = 4000s$
		Data size in Kilobytes	
One	time series	11.8	24.1
	load spectrum	0.2	0.2
Two	time series	23.6	48.2
	load spectrum	0.2	0.3
Three	time series	35.4	72.3
	load spectrum	1.0	1.2
Three (2016 cells)	time series	71,366.4	145,756.8
	load spectrum	1,355.4	2,209.0

range around specific cells that influence the sensor value. For calculation of the sensor value either the mean, the maximum or minimum value of all cells in the measuring range is used.

In addition to the reduction of simulation data, this submodel—coupled with an optimization algorithm—is useful for the determination of thermistor placement. This allows the automatic placement of sensors at thermal hot-spots inside a battery system design.

G. Load Evaluation

As discussed in Section II-D, load-spectrum analysis is a suitable approach to determine and compare the magnitude of stress-factors on LIBs. The simulation framework uses a submodel for runtime load spectrum analysis, able to monitor single as well as combinations of any desired stress factors, published by some of the authors in [27]. The resulting statistical data can either be used as input for aging-models or processed into a numerical indicator for the stress by means of a weighted evaluation.

Load spectrum analysis significantly reduces the size of logging data while maintaining all information about aging-relevant events in the electrical and thermal state variables. An example is shown in Table II. A typical load cycle is simulated for different durations t_{sim} with a discrete time-step of $\Delta t = 1 \cdot 10^{-2} s$ and one, two or three system variables are either logged in a standard time-series format or evaluated in a load spectrum of the same dimension. The advantages become especially apparent when a system of 2016 individual LIBs are simulated, where a standard time-series approach would produce hundreds of megabytes of logging data.

For an even further reduction of the data size and a simplified comparison of different system designs a degradation indicator D can be introduced, offering a weighted valuation when operating parameters are in aging-relevant ranges. Table III shows an exemplary definition for calculation of the degradation indicator for cell temperatures. In the example, temperatures in the range 20-40 °C are considered as ideal and not relevant for excessive aging, consequently, as long as a cell's temperature is within this range the aging indicator is not incremented. If the temperature exceeds 40 °C, the time $t_{temp}(T)$ the cell stays at the respective temperature T is counted with a linearly increasing weighting factor $w_{temp}(T)$. If the temperature exceeds 60 °C, the temperature is considered as damaging, expressed by a proliferated and exponentially increasing $w_{temp}(T)$. The analogous process also applies to all other aging-relevant operating parameters.

At the end of a simulation the total degradation indicators

$$D = \sum_{\text{time-steps}} t_{temp}(T)\ w_{temp}(T) \tag{24}$$

from simulation with different load cycles of cooling parameters can be compared and ranked according to their aging-potential. However, while this approach dismisses all aging information it is suitable to identify possible overloading of cells, especially with strictly chosen weighting factors.

H. Reference Implementation

A reference implementation was done in MATLAB®/ Simulink®. The complete simulation framework is available under an open-source license[1].

IV. PARAMETERIZATION AND VALIDATION

This section describes the electrical and thermal validation of the simulation framework on the cell and the system level.

A. Electrical Submodel on the Cell Level

First, parameterization and validation is performed on the cell level. For the measurement setup cylindrical 18650 cells of the type Panasonic NCR18650PF with a nominal capacity of 2.9 Ah were used. In order to provoke strong compensating currents between the cells for the subsequent system validation, two cells—cell A and B—with different aging stages were selected for parameterization of the simulation model.

[1] https://github.com/TUMFTM/sim_battery_system

TABLE III: EXEMPLARY WEIGHTING FACTOR FOR CELL TEMPERATURE.

Weighting factor $\mathbf{w_{temp}(T)}$	0	0	0	0	0.2	0.4	0.6	0.8	10	20	40	160
Temperature in °C	20	25	30	35	40	45	50	55	60	65	70	75
Temperature range	**ideal**				**transition**				**damaging**			

Both cells were characterized by a pseudo-static OCV measurement with a current of C/50 for capacity determination with a full constant current constant voltage (CCCV) discharge cycle between the cut-off voltages 4.2 V and 2.5 V. Afterwards, a HPPC was carried out in steps every 10% SOC for impedance fitting. The tests show a remaining capacity of 2.769 Ah and 2.336 Ah for cell A and B, respectively. For validation, a complete CCCV charge step with C/2 and the dynamic stress test (DST), repeated from a full charge until the lower cut-off voltage is reached, were performed. The results are shown in Figure 3.

For both cells the model shows a low overall voltage error despite their different aging stages. In general, model performance is increased with enhanced system dynamics as can be seen by comparing the voltage error during CCCV charge and dynamic DST cycling with up to 200 mV and less than 20 mV, respectively. As expected, low SOC ranges remain challenging for pulse fitted ECM models, which explains the lower accuracy at the beginning of the charge cycle and end of the DST cycle. However, single cell model validity is proven over the operational range.

B. Measurement of Compensating Currents

In order to measure the current distribution of parallel connected cells on the system level, inter-cell connectors and a current sensor are added to form serial cell strings. For the cell string HILUMIN® straps are spot-welded to both terminals of the LIBs. On the positive electrode's terminal, the HILUMIN® strap is soldered to a custom circuit board, including the hall effect current transducers. A schematic view of a cell string is shown in Figure 4. The individual cell strings are connected in parallel using a copper bus bar, shown in Figure 5. For subsequent work, the measurement setup can be extended to accommodate a higher amount of parallel connected cells.

To determine the magnitude of the ohmic shift due to connection resistances, which have to be regarded in the system model, different EIS measurements have been performed with two cells at 50 % SOC. An exploded assembly drawing of one parallel string in Figure 5 illustrates all occurring electrical connection resistances. In Figure 4, measurement points are marked as A_n-B_n, whereby the respective impedance Z_n is measured. The measured impedance spectra for one cell are plotted in Figure 6 (left). From the impedance Z_1 of two cells, the ideal parallel connection without additional impedance by the test bench can be calculated analytically for every frequency [22]. This result can be compared with the impedance spectrum of the final parallel connection. Ideal and measured impedance spectra of the parallel connection are shown in Figure 6 (right).

C. Electrical Submodel on the System Level

The measurement of the parallel connection of both cells and the model response is illustrated in Figure 7. The left hand side figure shows the complete CCCV charge with a slight error during current ramp-up, which is caused by the aforementioned accuracy limitation of ECMs at low SOC ranges. Consequently, simulated balancing currents of both cells match the measurement, except for a significant deviation at the beginning of charging. The overall error during CCCV remains within a range of ±40 mV and a current error less than 200 mA. Model response during dynamic DST cycling is given in the right hand side figure. Here, the model closly follows the measurement over the whole cycle. The voltage error stays within ±20 mV, the associated current error is less than 60 mA. Both validation cycles prove the validity of the electrical model on the system level and enable further assessment of bigger cell units connected in serial and parallel.

D. Thermal Submodel

While many approaches for the validation of thermal cell models have been presented in literature [29], [32]–[35], the parameterization of the thermal submodel on the system level poses a great challenge. The heat fluxes between the cells and to the environment cannot easily be distinguished, since only the resulting cell temperatures can be measured. So even if the LIBs' heat generation on the cell level is known, the impact of the additional effects on the system level and unknown heat transfer paths impede an analytical determination of the overall thermal properties. Furthermore, because of the interdependence of the electrical and the thermal cell behavior, if any of the electrical and thermal LIB and system parameters are

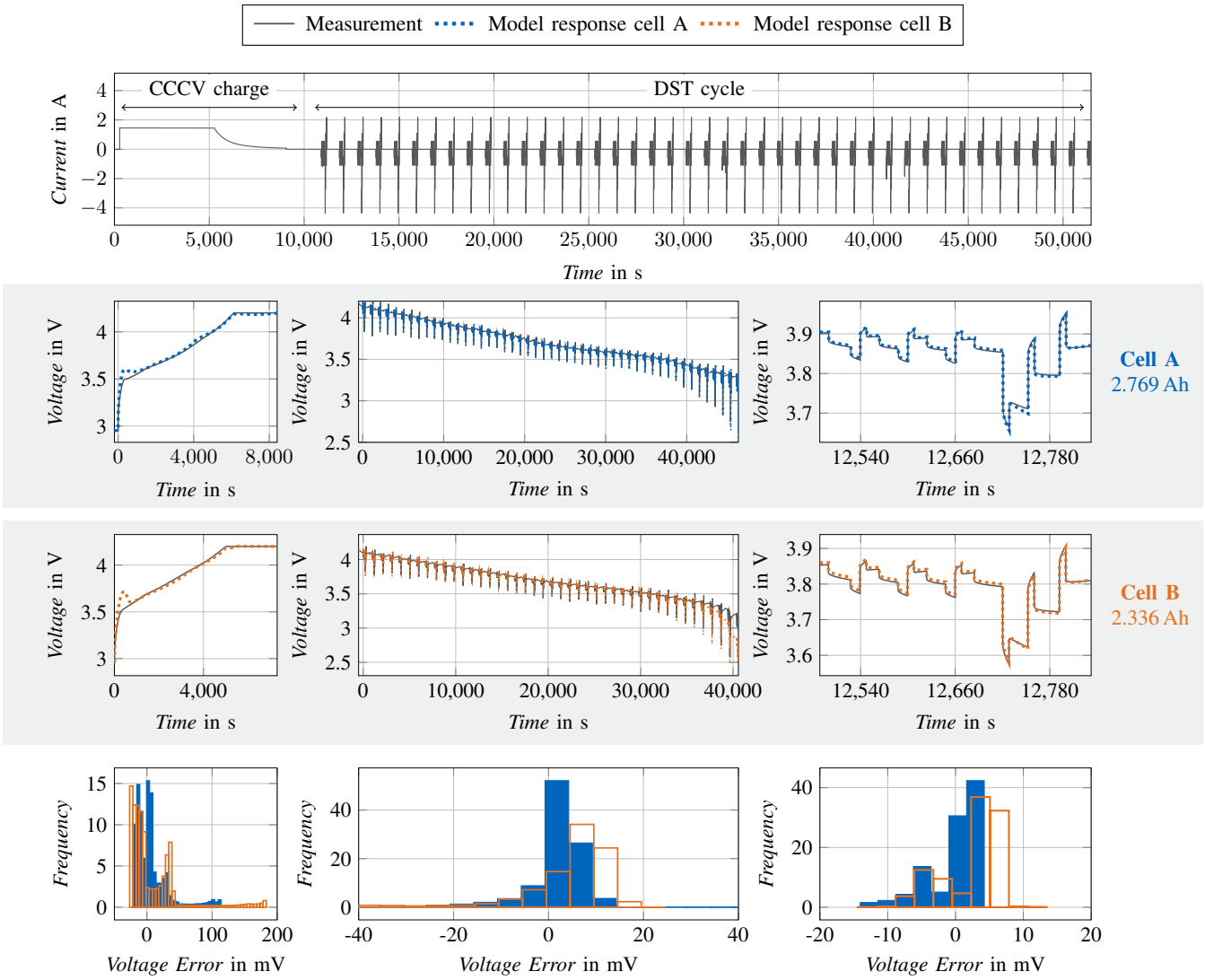

Fig. 3: Single cell validation for both employed 18650 LIBs over the mixed validation cycle. From top to bottom: Applied current profile of the mixed validation cycle, single cell voltage measurement compared to model response in CCCV phase, overall DST and a single DST repetition for cell 1 and cell 2, voltage error histogram of measurement and model response of both cells.

incorrect, the individual cell current and heat production are simulated inaccurately, with limited possibilities to identify the origin of the error.

These considerations lead to the conclusion that the parameterization process needs to be supported by an optimization approach that—assuming accurate electrical and thermal modelling at the cell level—determines the conductive and convective heat transfer on the system level. An optimization approach based on the non-linear least squares method was implemented and in a preliminary test was used to determine the thermal system parameters for a simulated battery system consisting of nine cells in a 3x3 configuration using arbitrary convective and conductive heat transfer coefficients. For both the simulated system temperatures and the later optimization, it was assumed that heat flux only occurs between adjacent cells.

The optimization algorithm was able to obtain the correct thermal parameters for all tested battery system configurations reaching thermal equilibrium with different starting temperatures of the individual cells. An exemplary temperature profile is shown in Figure 8. The optimization was able to correctly determine the parameters for the thermal system for all tested convective and conductive heat transfer coefficients. This is also the case for other system configurations using more cells and other layouts, even if the initial parameter values for the optimization differed in orders of magnitude from the correct one. The only requirement for a successful parameterization was that both convective and conductive heat transfer effects

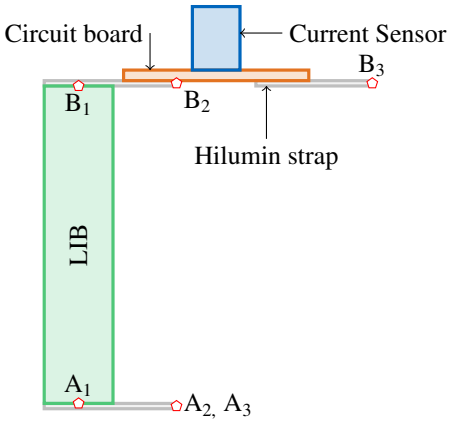

Fig. 4: Schematic view of a cell string for separate current tracking.

are present in the temperature profile. In Figure 8, this is visible in the first 50 s, when conduction between the cells is the dominant heat transport mechanism. After the temperatures in the system approach equalization, convective heat transfer to the environment becomes the predominant mechanism. Therefore, for tests with real battery systems it seems expedient to generate temperature gradients between the cells by means of selective heating or cooling.

First tests with a real 12s battery module built from prismatic cells from a production vehicle with an imposed temperature gradient by cycling one cell in the middle of system showed a comparable temperature profile to the one used for testing the optimization algorithm. Therefore, it is suspected that the presented approach of model parameterization using a thermal equalization test with different starting temperatures of the individual LIBs can be used for real system parameterization of larger battery systems. However, fluctuations around the target temperature and uneven heat dissipation due to air turbulence in the climatic chamber used for the tests influenced the temperature profile and made a final verification of the method unfeasible in the scope of this paper.

Therefore, in the future the authors will undertake further research and improvements of the measurement setup to reach the goal of global model validity.

V. Discussion

The intended purpose of the simulation framework was the electrical and thermal concept development and the aging simulation of automotive battery systems. These use-cases require the simulation of large battery systems with a high number of individual cells and cover a long time-frame. The framework was also designed to be able to adapt to different LIB types with only a minimum of parameterization required. To achieve this, several simplifications are necessary.

The electrical submodel is based on an ECM with four RC elements. While ECMs can only approximate real cell dynamics, this approach has been found to be sufficiently accurate by many studies. The literature review in Subsection II-B showed that no ECM higher that the fourth order has been used so far for system simulation. Thus, compared to other approaches, a high accuracy on the cell level can be assumed and has been shown in the validation. Only small divergences between simulation and measurment occur at low SOC levels. This high accuracy is needed, because on the system level due to the complex interaction between the cells, even slight deviations of the simulated compared to the real cell behavior lead to significant divergences in the resulting currents. On the other hand, an ECM of the forth order, compared to less complex approaches, leads to a significantly increased computational demand. Especially for large battery systems with a high amount of individual LIBs it must be determined, whether the complex cell model is still feasible, or—at the cost of accuracy— the order of the ECM must be reduced. Due to the modular approach of the simulation framework the cell model can be easily adapted.

For the thermal simulation two approaches have been presented. The first approach assumed an only convective heat transfer from the cells to their environment without consideration of heat fluxes between the cells. If the simulated battery system shows a uniform temperature distribution and the LIBs are physically separated, this model representation may suffice. In this case, the advantages of a facilitated parameterization and computation—no interaction between the cells must be simulated—outnumber the drawbacks in accuracy of this substantial simplification of the real circumstances.

In many cases, however, the heat fluxes between the cells contribute substantially to the thermal system behavior and cannot be ignored. Usually in battery systems built from prismatic or pouch type LIBs, the cells are in direct physical contact and cooling measures are only in place at specific parts inside the system making heat exchange between the cells a determining part of the operating behavior. Consequently, the model is designed to simulate heat fluxes between all cells inside the battery system. However, to reduce complexity, the optimization approach to parameterize the model currently only assumes heat fluxes between LIBs directly adjacent. If heat fluxes occur across multiple cells—e.g. caused by

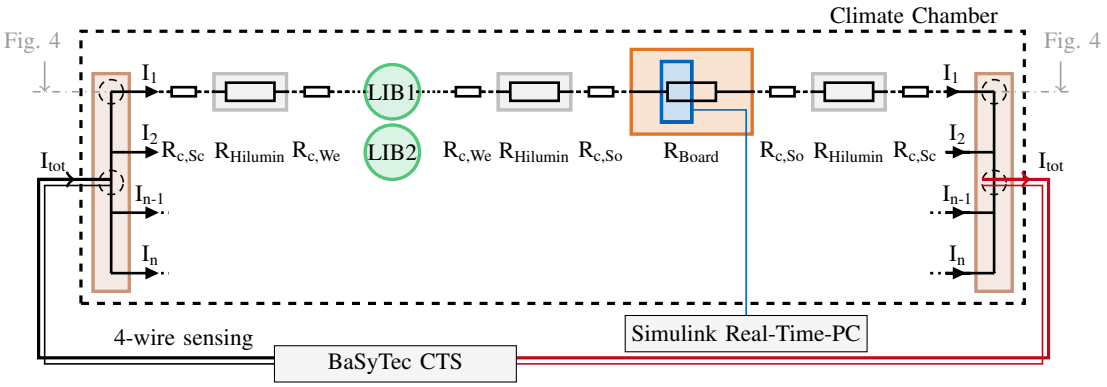

Fig. 5: Schematic view of one cylindrical 18650 cell including electrical connection (resistance welded Hilumin strap), circuit board with current-sensor (soldered to hilumin straps) and copper bus bar for inter-cell connection (screw connection).

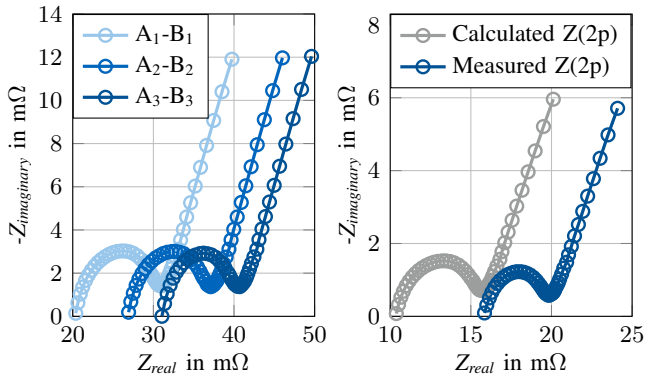

Fig. 6: Left: Extract of 2p validation with CCCV charge. Right: DST repetition at 50% SOC.

the enclosure or electrical wiring—further development regarding the optimization approach is necessary.

The simulation model intentionally does not include a dedicated aging model to maintain maximum general applicability. Aging simulation requires extensive testing and aging models must be tailored to the later use case, and the relevant stress factors [27]. Nevertheless, in order to be able to make statements about the electrical and thermal load, a load-evaluation subsystem based on load-spectrum analysis has been proposed. While the method itself does not assess aging but only shows how long or often the system's operation parameters are within specific ranges, the introduced degradation indicator (Subsection III-G) aims to weight the system load according to its severity. Currently, the weighting factors are defined according to established design goals, so no direct proportionality to real cell aging exists. Still, the degradation indicator is an auspicious approach to identify overload of the system.

VI. Conclusion and Outlook

This paper proposed a holistic simulation framework to assess electrical and thermal loads in lithium-ion battery systems. The ECM-based cell model—derived from an extensive literature research—is expanded to represent serial and parallel connections using an analytic approach. A thermal model simulates reversible and irreversible heat losses of the individual LIBs that are modelled as lumped masses. On the system level the model allows the simulation of heat dissipation to the cell's surroundings—e.g. a cooling system—and heat fluxes between the cells caused by thermal gradients between the cells.

To reduce the amount of logging data and to account for the conditions in real battery systems, where not all LIBs may be monitored, a temperature sensor model was developed allowing any desired placement of sensors inside the battery system. Furthermore, a load-evaluation subroutine is included to assess cell and system load and optionally compute scalar ratios, rating the system load.

The electrical part of the model was validated on the cell and the system level and the challenges were discussed. An approach for the complex parameterization of the thermal model was presented and its plausibility was evaluated by simulation. In the course of the validation attempt using a real battery system, harmful side effects from the used measurement setup were identified, impeding final validation.

The model-based approach of the reference implementation in MATLAB®/Simulink® allows straightforward expansion of the simulation framework and its submodels. Due to the open-source licensing the complete simulation framework is available to the public (https://github.com/TUMFTM/sim_battery_system).

In future work, the authors will refine the thermal

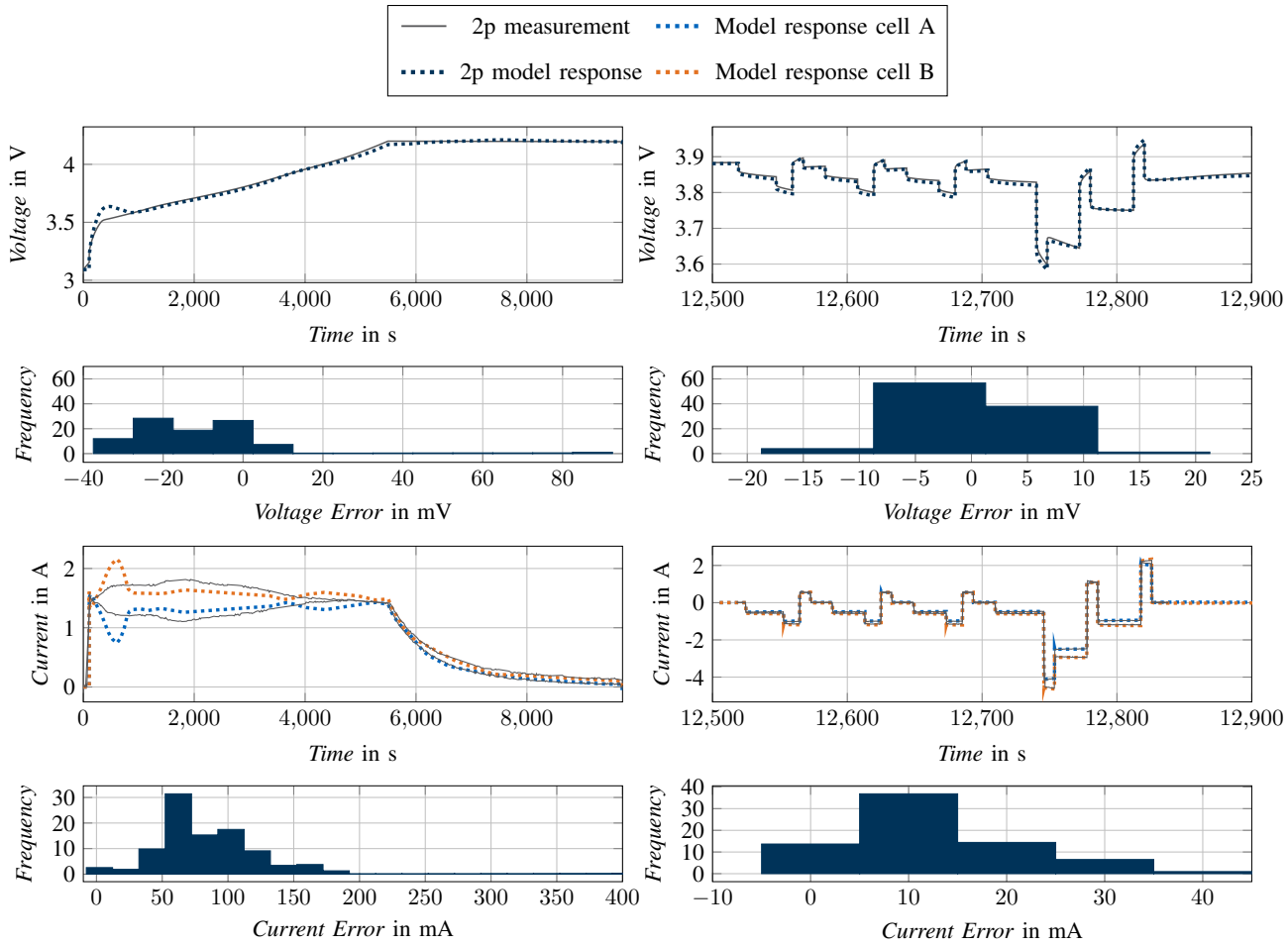

Fig. 7: Extract of 2p validation with CCCV charge (left) and single DST repetition (right).

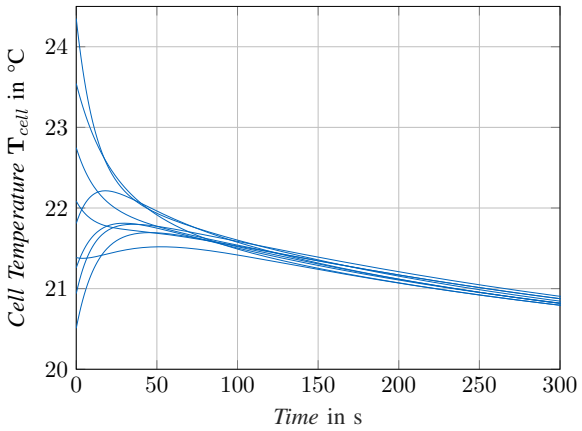

Fig. 8: Extract of the temperature distribution for a battery system of nine prismatic cells arranged in a 3x3 matrix achieving thermal equilibrium.
Thermal parameters used: $\mathbf{T}_\infty$=20 °C, $R_{\alpha,x}$=12 m^{2}K/W, $R_{\alpha,y}$=30 m^{2}K/W, $R_{\alpha,z}$=80 m^{2}K/W, $R_{\lambda,x}$=1.2 m^{2}K/W, $R_{\lambda,x}$=8.13 m^{2}K/W, $R_{\lambda,x}$=3.77 m^{2}K/W.

measurement setup to achieve global validity of the simulation model for both the electrical and thermal parts and for different cell types on the system level. In this context also the electrical parameterization approach will be refined and tested for larger parallel interconnections.

Acknowledgement

The authors want to thank the following persons for their contributions to the simulation framework:

Michael Baumann (M.B.) contributed to the ECM modeling and the electric parameterization and validation as part of his PhD-Thesis. He also consulted the authors on characterization and validation measurements on the cell and the system level.

André Thomaser (A.T.) contributed to the development and implementation of the thermal submodel (Subsection III-D), the stability calculation (Subsectin III-E) and the optimization of the thermal model (Subsection IV-D) as part of his bachelor thesis.

Sebastian Huber (S.H.) contributed to the development

and implementation of the temperature sensor submodel (Subsection III-F) as part of his term project.

Thilo Wurster (T.W.) contributed to the implementation of the allocation of different ECM parameter sets (Subsection III-A) to their numeric representation in the simulation framework as part of his master's thesis.

The authors also want to thank the Bavarian Research Foundation that funded parts of the research as part of the project *NEmo – Nutzerorientierte Elektromobilität [user-oriented electromobility]* (AZ-1203-16) and the Bavarian Ministry of Economic Affairs, Regional Development and Energy for funding the project *bawaii – battery analytics with artificial intelligence* (IUK-1808-0013).

Contributions

C.R. is the first and main author. He developed the structure of the simulation framework and researched and selected the underlying concepts. He also researched and developed the parameterization of the thermal system model and supported and advised the work of T.K., J.D., A.T., S.H. and T.W. He verified and finalized the implementation of the simulation framework.

L.W. is the second author. He researched the state of the art of existing models. Together with M.B. he is responsible for the parameterization algorithm of the ECM. Further he performed validation measurements of the electrical submodel on cell and on system level.

N.W. is the third author and contributed the analysis, validation and evaluation of the electrical submodel on cell and system level together with L.W..

T.K. researched and implemented the methods for load evaluation presented in Subsection III-G.

J.D. implemented the basic model structure, and researched and implemented the simulation of the serial and parallel connection (Subsection III-B) and the basic thermal submodel (Subsection III-C).

M.L. made an essential contribution to the conception of the research project. He critically revised the paper for important intellectual content. M.L. gave final approval of the version to be published and agrees to all aspects of the work. As a guarantor, he accepts responsibility for the overall integrity of the paper.

Abbreviations

BMS	battery management system
C-rate	electric current rate
CC	constant current
CCCV	constant current constant voltage
DST	dynamic stress test
ECM	equivalent circuit model
EIS	electrochem. impedance spectroscopy
FUDS	federal urban driving cycle
HPPC	high power pulse characterization
LIB	lithium-ion battery
OCV	open-circuit voltage
SEI	solid electrolyte interphase
SOC	state-of-charge

References

[1] Wladislaw Waag, Stefan Käbitz, and Dirk Uwe Sauer. Experimental investigation of the lithium-ion battery impedance characteristic at various conditions and aging states and its influence on the application. *Applied Energy*, 102:885–897, 2013.

[2] Andreas Jossen. Fundamentals of battery dynamics. *Journal of Power Sources*, 154(2):530–538, 2006.

[3] M. Broussely, Ph. Biensan, F. Bonhomme, Ph. Blanchard, S. Herreyre, K. Nechev, and R. J. Staniewicz. Main aging mechanisms in li ion batteries. *Journal of Power Sources*, 146(1-2):90–96, 2005.

[4] Seyed Mohammad Rezvanizaniani, Zongchang Liu, Yan Chen, and Jay Lee. Review and recent advances in battery health monitoring and prognostics technologies for electric vehicle (ev) safety and mobility. *Journal of Power Sources*, 256:110–124, 2014.

[5] Heinz Wenzl, Ian Baring-Gould, Rudi Kaiser, Bor Yann Liaw, Per Lundsager, Jim Manwell, Alan Ruddell, and Vojtech Svoboda. Life prediction of batteries for selecting the technically most suitable and cost effective battery. *Journal of Power Sources*, 144(2):373–384, 2005.

[6] Michael Baumann, Leo Wildfeuer, Stephan Rohr, and Markus Lienkamp. Parameter variations within li-ion battery packs – theoretical investigations and experimental quantification. *Journal of Energy Storage*, 18:295–307, 2018.

[7] Christoph Reiter, Nikolaos Wassiliadis, Leo Wildfeuer, Thilo Wurster, and Markus Lienkamp. Range extension of electric vehicles through improved battery capacity utilization: Potentials, risks and strategies. In *2018 21st International Conference on Intelligent Transportation Systems (ITSC)*, pages 321–326. IEEE, 2018.

[8] Mao-Sung Wu, Chang-Yen Lin, Yung-Yun Wang, Chi-Chao Wan, and C. R. Yang. Numerical simulation for the discharge behaviors of batteries in series and/or parallel-connected battery pack. *Electrochimica Acta*, 52(3):1349–1357, 2006.

[9] Gregory J. Offer, Vladimir Yufit, David A. Howey, Billy Wu, and Nigel P. Brandon. Module design and fault diagnosis in electric vehicle batteries. *Journal of Power Sources*, 206:383–392, 2012.

[10] Rob Spurrett, Carl Thwaite, Adam Holland, David Lizius, and Geoff Dudley. Modelling of highly-parallel lithium-ion batteries. *ESA SP*, pages 685–691, 2002.

[11] Fuqiang An, Jun Huang, Chengyu Wang, Zhe Li, Jianbo Zhang, Sean Wang, and Ping Li. Cell sorting for parallel lithium-ion battery systems: Evaluation based on an electric circuit model. *Journal of Energy Storage*, 6:195–203, 2016.

[12] So Miyatake, Yoshihiko Susuki, Takashi Hikihara, Syuichi Itoh, and Kenichi Tanaka. Discharge characteristics of multicell lithium-ion battery with nonuniform cells. *Journal of Power Sources*, 241:736–743, 2013.

[13] Matthieu Dubarry, Arnaud Devie, and Bor Yann Liaw. Cell-balancing currents in parallel strings of a battery system. *Journal of Power Sources*, 321:36–46, 2016.

[14] Wei Shi, Xiaosong Hu, Chao Jin, Jiuchun Jiang, Yanru Zhang, and Tony Yip. Effects of imbalanced currents on large-format lifepo4/graphite batteries systems connected in parallel. *Journal of Power Sources*, 313:198–204, 2016.

[15] X. Gong, R. Xiong, and C. C. Mi. Study of the characteristics of battery packs in electric vehicles with parallel-connected lithium-ion battery cells. *IEEE Transactions on Industry Applications*, 51(2):1872–1879, 2015.

[16] Limei Wang, Yong Cheng, and Xiuliang Zhao. A lifepo4 battery pack capacity estimation approach considering in-parallel cell safety in electric vehicles. *Applied Energy*, 142:293–302, 2015.

[17] H. Zhang, T. Wang, R. Lu, C. Zhu, and Y. Zhao, editors. *Study on the Impedance Increase Fault of Parallel Connected Batteries Based on Simscape Model Simulation: Vehicle Power and Propulsion Conference (VPPC), 2015 IEEE*, 2015.

[18] Andrea Cordoba-Arenas, Simona Onori, and Giorgio Rizzoni. A control-oriented lithium-ion battery pack model for plug-in hybrid electric vehicle cycle-life studies and system design with consideration of health management. *Journal of Power Sources*, 279:791–808, 2015.

[19] Matthias Fleckenstein, Oliver Bohlen, Michael A. Roscher, and Bernard Bäker. Current density and state of charge inhomogeneities in li-ion battery cells with lifepo4 as cathode material due to temperature gradients. *Journal of Power Sources*, 196(10):4769–4778, 2011.

[20] Steven Neupert and Julia Kowal. Inhomogeneities in battery packs. *World Electric Vehicle Journal*, 9(2):20, 2018.

[21] Thomas Bruen and James Marco. Modelling and experimental evaluation of parallel connected lithium ion cells for an electric vehicle battery system. *Journal of Power Sources*, 310:91–101, 2016.

[22] Martin J. Brand, Markus H. Hofmann, Marco Steinhardt, Simon F. Schuster, and Andreas Jossen. Current distribution within parallel-connected battery cells. *Journal of Power Sources*, 334:202–212, 2016.

[23] Matthias Fleckenstein, Oliver Bohlen, and Bernard Bäker. Aging effect of temperature gradients in li-ion cells experimental and simulative investigations and the consequences on thermal battery management. *World Electric Vehicle Journal*, 5(2):322–333, 2012.

[24] Hannes Hopp. *Thermomanagement von Hochleistungsfahrzeug-Traktionsbatterien anhand gekoppelter Simulationsmodelle*. Research. Springer Vieweg, Wiesbaden, 2016.

[25] Rajib Mahamud and Chanwoo Park. Spatial-resolution, lumped-capacitance thermal model for cylindrical li-ion batteries under high biot number conditions. *Applied Mathematical Modelling*, 37(5):2787–2801, 2013.

[26] Anthony Barré, Benjamin Deguilhem, Sébastien Grolleau, Mathias Gérard, Frédéric Suard, and Delphine Riu. A review on lithium-ion battery ageing mechanisms and estimations for automotive applications. *Journal of Power Sources*, 241:680–689, 2013.

[27] Tanja Gewald, Christoph Reiter, Xue Lin, Michael Baumann, Thilo Krahl, Alexander Hahn, and Markus Lienkamp. Characterization and concept validation of lithium-ion batteries in automotive applications by load spectrum analysis. In *31st International Electric Vehicles Symposium & Exhibition (EVS 31) & International Electric Vehicle Technology Conference (EVTeC)*, Kobe, Japan, 2018.

[28] Mark Verbrugge. Adaptive, multi-parameter battery state estimator with optimized time-weighting factors. *Journal of Applied Electrochemistry*, 37(5):605–616, 2007.

[29] Akram Eddahech, Olivier Briat, and Jean-Michel Vinassa. Thermal characterization of a high-power lithium-ion battery: Potentiometric and calorimetric measurement of entropy changes. *Energy*, 61:432–439, 2013.

[30] Christoph Reiter, Xue Lin, Lars-Eric Schlereth, and Markus Lienkamp. Finding the ideal automotive battery concept: A model-based approach on cell selection, modularization and thermal management. *Forschung im Ingenieurwesen*, 2019. Forthcoming.

[31] Abbas Tourani, Peter White, and Paul Ivey. Analysis of electric and thermal behaviour of lithium-ion cells in realistic driving cycles. *Journal of Power Sources*, 268:301–314, 2014.

[32] Yasir Abdul-Quadir, Tomi Laurila, Juha Karppinen, and Mervi Paulasto-Kröckel. Thermal simulation of high-power li-ion battery with limn1/3ni1/3co1/3o2 cathode on cell and module levels. *International Journal of Energy Research*, 38(5):564–572, 2014.

[33] Christophe Forgez, Dinh Vinh Do, Guy Friedrich, Mathieu Morcrette, and Charles Delacourt. Thermal modeling of a cylindrical lifepo4/graphite lithium-ion battery. *Journal of Power Sources*, 195(9):2961–2968, 2010.

[34] Elham Hosseinzadeh, Ronny Genieser, Daniel Worwood, Anup Barai, James Marco, and Paul Jennings. A systematic approach for electrochemical-thermal modelling of a large format lithium-ion battery for electric vehicle application. *Journal of Power Sources*, 382:77–94, 2018.

[35] Jiuchun Jiang, Haijun Ruan, Bingxiang Sun, Weige Zhang, Wenzhong Gao, Yi Le Wang, and Linjing Zhang. A reduced low-temperature electro-thermal coupled model for lithium-ion batteries. *Applied Energy*, 177:804–816, 2016.